

Fabrication of Magnesium-Carbonate Apatite by Conventional Sintering and Spark Plasma Sintering for Orthopedic Implant Applications

(Fabrikasi Magnesium-Karbonat Apatit oleh Pensinteran Konvensional dan Pensinteran Percikan Plasma untuk Aplikasi Implan Ortopedik)

IWAN SETYADI^{1,2}, TOTO SUDIRO³, BAMBANG HERMANTO³, PRIMA RIZKY OKTARI⁴, ACHMAD FAUZI KAMAL⁴, AHMAD JABIR RAHYUSSALIM⁴, BAMBANG SUHARNO⁵ & SUGENG SUPRIADI⁶

¹*Department of Metallurgical and Materials Engineering, Faculty of Engineering, Universitas Indonesia, Depok, I 16424, Indonesia*

²*Center for Material Technology, Agency for the Assessment and Application of Technology (BPPT)-Indonesia*

³*Research Center for Physics (P2Fisika), Indonesian Institute of Sciences (LIPI), Indonesia*

⁴*Department Orthopedic and Traumatology, Faculty of Medicine, Universitas Indonesia, Indonesia*

⁵*Department of Metallurgical and Materials Engineering, Faculty of Engineering, Universitas Indonesia, Indonesia*

⁶*Department of Mechanical Engineering, Universitas Indonesia, Indonesia*

Received: 27 April 2021/Accepted: 15 August 2021

ABSTRACT

Magnesium-Carbonate Apatite (Mg-xCA) is one of the potential magnesium composites to be developed as an alternative biodegradable implant material. Several attempts were made to optimize its characteristics. In this study, Mg-xCA ($x = 0, 5, 10,$ and 15% wt) was prepared by powder metallurgy through warm compaction (WC) and further densified by 2 sintering process methods, namely conventional sintering (CS) and spark plasma sintering (SPS). The characterization included density test, XRD test, microstructure test (OM and SEM-EDS-Mapping), microhardness test, and electrochemical test. The SPS process improves the characteristics of Mg-xCA better than the CS process. The SPS process can increase the relative density by about 0.7-2.4%, increase the hardness by about 2-13%, and reduce the corrosion rate by about 32-49% compared to the initial condition before sintering (WC). The SPS structure has a lower oxygen elemental content than the CS structure. The sintered process with SPS is considered effective for the fabrication of Mg-xCA powder-based composites compared to the CS process.

Keywords: Characterization; conventional sintering; magnesium-carbonate apatite; spark plasma sintering

ABSTRAK

Magnesium-Karbonat Apatit (Mg-xCA) adalah salah satu komposit magnesium yang berpotensi untuk dikembangkan sebagai bahan implan biodegradasi alternatif. Beberapa usaha dilakukan untuk mengoptimalkan ciri-cirinya. Dalam kajian ini, Mg-xCA ($x = 0, 5, 10,$ dan 15% wt) disiapkan oleh metalurgi serbuk melalui pepadatan suam (WC) dan selanjutnya diperkecilkan dengan 2 kaedah proses pensinteran, iaitu pensinteran konvensional (CS) dan percikan plasma pensinteran (SPS). Pencirian tersebut merangkumi ujian kepadatan, ujian XRD, ujian struktur mikro (OM dan SEM-EDS-Pemetaan), ujian kekerasan mikro dan ujian elektrokimia. Proses SPS meningkatkan ciri Mg-xCA lebih baik daripada proses CS. Proses SPS dapat meningkatkan ketumpatan relatif sekitar 0.7-2.4%, meningkatkan kekerasan sekitar 2-13% dan mengurangkan kadar kakisan sekitar 32-49% dibandingkan dengan keadaan awal sebelum pensinteran (WC). Struktur SPS mempunyai kandungan unsur oksigen yang lebih rendah daripada struktur CS. Proses pensinteran dengan SPS dianggap berkesan untuk pembuatan komposit berasaskan serbuk Mg-xCA berbanding dengan proses CS.

Kata kunci: Magnesium-karbonat apatit; pencirian; pensinteran konvensional; pensinteran plasma percikan

INTRODUCTION

Magnesium is one of the most widely used elements as the basis for developing biodegradable bone implant material. Its superior nature: lightweight, biocompatible, has a bone-like elastic modulus, and has a high toxicity limit in the body (Godavitarne et al. 2017; Gu & Zheng 2010; Haghshenas 2017; Kuśnierczyk et al. 2017; Siska Wiwanto et al. 2018; Supriadi et al. 2018) make it as a first choice. However, to be applied it needs improvement efforts particularly related to mechanical properties and degradation rates. One of the efforts being developed to increase the capability of magnesium is by forming a new structure, namely the magnesium composite (Zheng et al. 2014).

Potential reinforcement types used include bioceramics based on calcium phosphate, such as hydroxyapatite (HA) which has been previously studied in Mg-HA composite fabrication. Several previous studies on the Mg-HA sintering process reported that the lowest corrosion rate (CR) was 2.09 mm/y or corrosion current density (I_{corr}) $1.0E-04 \text{ Acm}^{-2}$ in SBF at Mg-10HA as a result of the combination of powder metallurgy (PM) and microwave sintering (MS) (Xiong et al. 2016), CR of 5.44 mm/y in 3.5% NaCl solution at lamellar Mg-10HA as a result of PM and SPS (Sunil et al. 2014). Meanwhile, in the study of the sintering process (CS and SPS) of Mg-10HA, it was reported that there was a decrease in the release of Mg ions by the SPS process compared to CS. The release of Mg ions was 85% (CS) and 45% (SPS) after 28 days of immersion in Simulated Body Fluid (SBF) (Mohammad et al. 2020). Another studies with the fabrication process through a combination of PM and extrusion were also reported that the lowest CR or I_{corr} was 1.27 mm/y or $6.002E-05 \text{ Acm}^{-2}$ in SBF at Mg-10HA (Gu et al. 2010), 1.25 mm/y in artificial sea water at AZ91D-20HA (Witte et al. 2007) and about 15 mm/y after immersion for 96 h in Phosphate Buffered Saline (PBS) solution at Mg-5CA (Campo et al. 2014).

Carbonate Apatite (CO_3Ap ; $\text{Ca}_{10-a}(\text{PO}_4)_{6-b}(\text{CO}_3)_c(\text{OH})_{2-d}$) is a bioceramic type based on calcium phosphate, such as hydroxyapatite (HA). CA has the same properties as HA: biocompatibility, bioactivity, and bioresorption (Ahmad Jabir et al. 2019; Godavitarne et al. 2017; Kuśnierczyk et al. 2017; Radha & Sreekanth 2017; Youness et al. 2017), however, CA is considered to have more potential for bone healing, particularly CA (type B), because it is more easily absorbed than HA (Ayukawa et al. 2015; Ishikawa 2019) and promotes bone formation (osteoconductivity). Previous researcher's studies show the absorption of CA and the formation

of new bone tissue without the fibrotic tissue formation as in HA (Ayukawa et al. 2015; Hirokazu et al. 2015; Masayuki et al. 2017).

In CA (type B) some of the PO_4^{3-} clusters in HA are replaced by carbonates (CO_3^{2-}) (Ahmad Jabir et al. 2019; Atmaja Surbakti et al. 2017; Kuśnierczyk et al. 2017; Landi et al. 2003; Linhart et al. 2000; Madupalli et al. 2017). However, according to Doi et al. (1995), starting at 50 °C, CO_3^{2-} decomposes into CO_2 gas and tends to increase at 450-650 °C.

Further densification process of the Mg-based composite becomes an important part of the development stage. Densification can be done through a sintering process (Annur 2017; Iwan Setyadi et al. 2020; Xiong et al. 2016) or with a plastic deformation mechanism (Del Campo et al. 2017, 2014; Supriadi et al. 2018; Witte et al. 2007). The sintering process can be carried out by 2 methods, namely conventional sintering (CS) processes, such as sintering with vacuum tube furnace (Annur et al. 2017; Iwan Setyadi et al. 2020) and unconventional sintered processes such as spark plasma sintering (SPS) (Khodaei et al. 2020; Liu et al. 2019) and microwave sintering (Xiong et al. 2016). The SPS process has more potential for the Mg composite densification process than MS. The SPS process has advantages. The SPS process utilizes a concentrated and uniform microplasma discharge between particles (plasma heating), the diffusion process (Joule heating) takes place in a short time (5-20 minutes), atmospheric conditions (vacuum) are regulated by the system so that the process is very clean, and at the same time a plastic deformation process takes place under uniaxial pressure (NN n.d.).

The results of previous studies show significant improvements in compressive strength and corrosion resistance on Mg-10% wt. HA composites resulting from SPS compared to CS results (Khodaei et al. 2020). A short SPS time reduces interactions and reactions that occur in HA and Mg particles so that the characteristics are significantly improved compared to CS.

However, the Mg densification process with sintering is conducted at high temperatures (450-550 °C) (Jaiswal et al. 2018; Khodaei et al. 2020; Xiong et al. 2016). This is a concern during the Mg-xCA densification process. Besides that, magnesium is a reactive element. Mg is flammable and its flashpoint temperature is 473 °C. This research is part of a research series on the development of Mg-xCA composites for biodegradable implant materials. In the early stages, the initial compaction of Mg-xCA with warm compacting was

developed and the initial development of the Mg-xCA miniplate (Iwan Setyadi et al. 2020a, 2020b). The next development stage is an effort to optimize the characteristics of Mg-xCA through further densification, one of which is the sintering process.

This study aims to improve the characteristics of Magnesium-Carbonate Apatite (Mg-xCA) for orthopedic implant material applications through further densification by sintering. Meanwhile, the objective of the study was to observe and determine the characteristics of Mg-xCA sintered by the CS process (using a vacuum tube furnace) and the SPS process. The objectives of the study were also to observe the effect of adding and increasing the CA content of sintered Mg-xCA. The observations included density, XRD, microstructure (OM, SEM-EDS-Mapping), microhardness (Hv), and biocorrosion test results.

MATERIALS AND METHODS

MATERIALS

The raw materials were commercial Mg powder (Merck KGaA, size 60-300 μm , purity: $\geq 99.9\%$) and local CA powder (size of $\pm 74 \mu\text{m}$). Mg & CA powders were mixed with a planetary ball mill (PM400-Retsch) for 5 hours at 200 RPM. Mg-xCA was made with 4 compositions, each $x = 0, 5, 10$ and 15% wt CA. CA composition referred to the composition of previous studies of Mg-xHA (Del Campo et al. 2014) and Mg-xCA (Ahmad Jabir et al. 2021; Iwan Setyadi et al. 2020) where generally the optimal results obtained were in the composition range of 0-15% wt. Optimal results refer to the lowest degradation rate, namely at Mg-5HA. Corrosion testing was carried out by immersing the sample in Phosphate Buffered Saline (BPS) solution (Del Campo et al. 2014).

CONVENTIONAL SINTERED PROCESSES

In the initial stage, the densification of Mg-xCA composite powder was conducted by a warm compaction (WC) process. The powder was put into a mold cavity (10 mm diameter) then heated in a muffle furnace to 330 °C (heating rate 10 °C/min) and pressed at 350 MPa with a punch (Iwan Setyadi et al. 2020).

Further densification with the CS process was conducted in a vacuum tube furnace (OTF 1200X, MTI Corporation) under vacuum ($P = -0.1 \text{ MPa}$) and an O_2 content $\leq 150 \text{ ppm}$. O_2 content was controlled by oxygen analysis (type EQ-W1000-LD, MTI Corporation). Heating was carried out to 200 °C (held for 10 minutes), then

heated again to 450 °C (held for 1 hour). The heating rate was 5 °C/min.

SPARK PLASMA SINTERING (SPS) PROCESS

Mg-xCA powder was inserted into the graphite mold cavity (diameter 20 mm, height 11 mm). The mold was put into the SPS (DR. Sinter) heating chamber. Initial chamber vacuum pressure of -4.4Pa. The heating was done up to 350 °C (heating rate 50 °C/min) then raised again to 400 °C (sintered temperature) and held for 15 min. Punch pressure 12.5 kN.

DENSITY TESTING

Density testing was done with a density meter (DH-300X). The test used Archimedes law and was carried out at 27 °C. The reported result was relative density (experimental density divided by theoretical density). The relative density calculation refers to the density of pure Mg and CA, where the respective values are 1.73 g/cm³ for pure Mg [10] and 3.24 g/cm³ for CA (Center for Material Technology (BPPT) 2017).

MICROSTRUCTURE OBSERVATIONS

Microstructure observations were conducted using an optical microscope (Meiji Techno). Observations were made on the cross-section of the rod. Sample preparation began with a grinding process using a grid of # 400 - # 2000 sandpaper. 1 μm alumina paste was used for polishing. The etching material used was 1.5 g of the picric acid solution, 25 mL of ethanol, 5 mL of acetic acid and 10 mL of distilled water (Del Campo et al. 2014).

To check the structure in more detail and analysis of its elements, scanning electron microscopy (SEM) testing, energy dispersive X-ray spectroscopy (EDS), and mapping were conducted using Phenom (magnification 160 - 350,000x) and Inspect F50 (magnification 14 - 1,000,000x).

XRD analysis (Rigaku-MiniFlex 600) diffractometer with $\text{CuK}\alpha$ radiation and a scan rate of 10 degrees/min was used for phase identification. XRD analysis used High Score Plus software.

MICROHARDNESS TESTING

Hardness testing was carried out on Mg-xCA samples for each fabrication process using the microindentation hardness method (ASTM E384-17 standard) ((ASTM E384-17) 2017). The microhardness test was conducted using the Hv microhardness test (Struers-DuraScan) at 5 measurement points in each sample. For Mg-based metal, the load used is 9.807 N (HV1).

BIOCORROSION OR DEGRADATION TESTING

The degradation (corrosion) tests were carried out using the potentiodynamics polarization method based on ASTM-G5-94 ((G5-94) 2014) and calculations referring to ASTM-G102-89 ((G102-89) 2015; Kingston Technical Software, n.d.). Corrosion rate testing was conducted by using an electrochemical station (Zahner Zennium X). There were 3 electrode cells which included a saturated calomel electrode as a reference electrode, platinum as a counter electrode, and sample as a working electrode. The testing process was conducted at 37 °C, pH 7.4 in SBF solution (Kokubo et al. 1990). The SBF composition

(capacity of 1 L) was NaCl (7.996 g), NaHCO₃ (0.350 g), KCl (0.224 g), K₂HPO₄·3H₂O (0.228 g), MgCl₂·6H₂O (0.305 g), 1M-HCl (40 mL), then about 90% of the total amount of HCl was added CaCl₂ (0.278 g), Na₂SO₄ (0.071g) and (CH₂OH) 3CNH₂ (6,057 g).

RESULTS AND DISCUSSION

RELATIVE DENSITY

The results of the Mg-xCA density test after being sintered respectively by CS and SPS are shown in Table 1.

TABLE 1. Relative density ($\rho_{\text{exp}}/\rho_{\text{theo}}$ (%)) Mg-xCA after being sintered with CS and SPS respectively. Mg-xCA before sintering (WC) is used as a comparison

Materials	WC		CS		SPS	
	ρ_{exp} (g/cm ³)	$\rho_{\text{exp}}/\rho_{\text{theo}}$ (%)	ρ_{exp} (g/cm ³)	$\rho_{\text{exp}}/\rho_{\text{theo}}$ (%)	ρ_{exp} (g/cm ³)	$\rho_{\text{exp}}/\rho_{\text{theo}}$ (%)
Mg-0CA	1.71	98.51	1.72	98.96	1.72	99.24
Mg-5CA	1.73	97.64	1.74	97.70	1.76	99.00
Mg-10CA	1.74	95.60	1.74	95.70	1.77	97.70
Mg-15CA	1.75	94.16	1.74	93.89	1.79	96.43

In Table 1 it can be seen that the relative density ($\rho_{\text{exp}}/\rho_{\text{theo}}$) of Mg-xCA sintered with SPS has increased 0.7 - 2.4% compared to the conditions before sintering (WC). The highest relative density value is at Mg-0CA (SPS) 99.24% and the lowest is at Mg-15CA (SPS) 96.3%. Meanwhile, not all CS results increased and some decreased, ranging from -0.3 - 0.5%. The lowest relative density of Mg-xCA (CS) is 93.89% at Mg-15CA.

The addition of CA in the Mg composite tends to reduce relative density. The more CA content, there is an indication of the formation of agglomeration and tends to decrease the relative density. This happens in both the CS process and the SPS process. However, the decrease in the relative density of the SPS process is less than the relative density of the CS process, particularly in the larger CA content (15% wt. CA). The phenomenon of a decrease in relative density due to the addition of reinforcement was also reported in the fabrication of Mg-HA with a content of 0, 5, 10 and 15% using the microwave sintering process of 99.4%, 98.1%, 96.5% and 93.4%, respectively (Xiong et al. 2016), as well as with other processes such as extrusion were 96.4%, 96.0 and 94%, respectively (Del Campo et al. 2014).

The relative density of the Mg-xCA SPS result is better than that of CS, due to the advantages of SPS technology. The temperature of the sinter is lower, which is 400 °C. Heating utilizes a micro-electric charge (can reach thousands of degrees C) which is focused and evenly distributed on the surface between the particles, so the temperature rises very rapidly and increases the diffusion between the particles. The heating process is short-lived (sinter time of 15 minutes) thus minimizing the decomposition of CA into CO₂ gas (Doi et al. 1995). The uniaxial pressure occurs simultaneously so that the density increases (NN n.d.). In addition, the chamber condition (oxidation and vacuum levels) is also maintained and controlled automatically by the system. The temperature also drops rapidly thereby minimizing heat propagation and grain growth.

Meanwhile, the conventional sintering process (CS) is carried out at a higher temperature (450 °C) and a long time (sintering 60 minutes) in a vacuum tube furnace. This high temperature and long time causes a decrease in the level of vacuum and the cleanliness of the tube space, thus opening the possibility of forming MgO and decarbonization of CO₃²⁻ in CA into CO₂ gas

as reported by Doi et al. (1995); Ishikawa (2019); Iwan Setyadi et al. (2020), particularly at temperatures of 450-650 °C. CO₂ gas can be trapped between Mg particles to form microporosity. This is the cause of a greater decrease in relative density at higher CA content, particularly Mg-15CA.

XRD RESULTS

The results of the Mg-xCA (CS and SPS) XRD test are shown in Figure 1. The MgO peak from the burned Mg is displayed as a comparison.

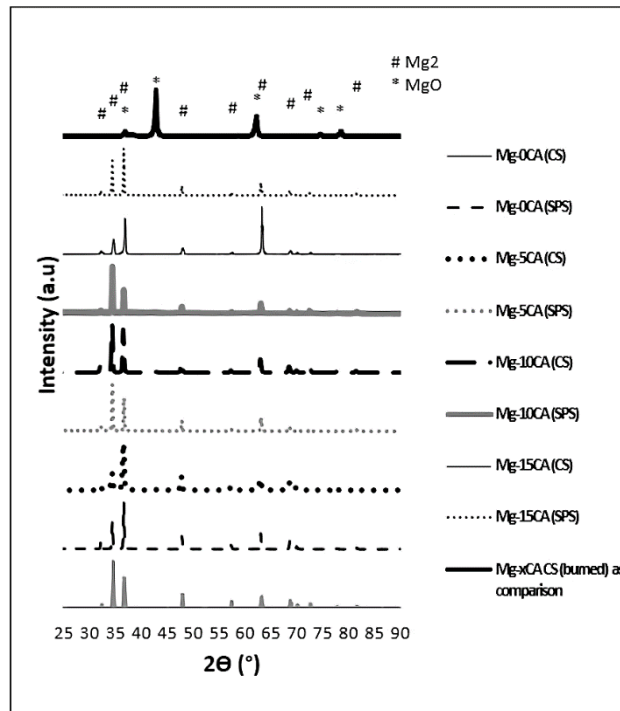


FIGURE 1. The XRD test results of Mg-xCA after being sintered with CS and SPS. The MgO peak from the burned Mg is displayed as a comparison

Referring to the XRD results (Figure 1), there are no other phases such as Mg-O in Mg-xCA (CS) or Mg-xCA (CS). No peak coincides with the example of the peak of burned Mg-xCA (CS) sample, particularly at $2\theta = 36.9, 42.84, 62.14, \text{ and } 74.58^\circ$. Peak Mg looks dominant, particularly at $2\theta = 32.1; 34.3; 36.5; 47.7; 57.3; 63; 68.5; 69.9; 72; 77.7 \text{ and } 81.5^\circ$. The sintering type only changes the Mg peak intensity particularly at $2\theta = 32.1; 34.3; 36.5^\circ$, while the appearance of peak CA is very small.

Further observations are conducted to determine the presence of elements or phases such as Mg, MgO, and CO₂ by high score plus software. The greater the CA content tends to increase the presence of these phases. The type of sintering process (CS and SPS) also influences the presence of these phases. In the SPS process, the appearance of CO₂ and MgO can be minimized, but not so in the CS process. The superiority of the SPS process

has also been reported on Mg-HA fabrication by previous researchers (Khodaei et al. 2020).

At XRD peak list of Mg-15CA (CS) (Figure 2) can be seen that CO₂ peaks (96-900-7890) are high, particularly at $2\theta = 32.3; 63.3; 63.4, 72.6, 77.9^\circ$ (indicated by the dashed line). These peaks also coincide with Mg peak (96-901-2435). In addition, on XRD result of Mg-15CA (CS) also is found the presence of MgO peaks (96-901-3243).

MICROSTRUCTURE OBSERVATIONS

OPTICAL MICROSCOPE/OM OBSERVATION

Figure 3 (Optical Microscope/OM observation) shows the shape and grain size of the Mg-xCA sample from CS and SPS results as well as before CS (as WC) almost the same. Its grain size is in the range 60-300 μm such as the initial size of Mg powder.

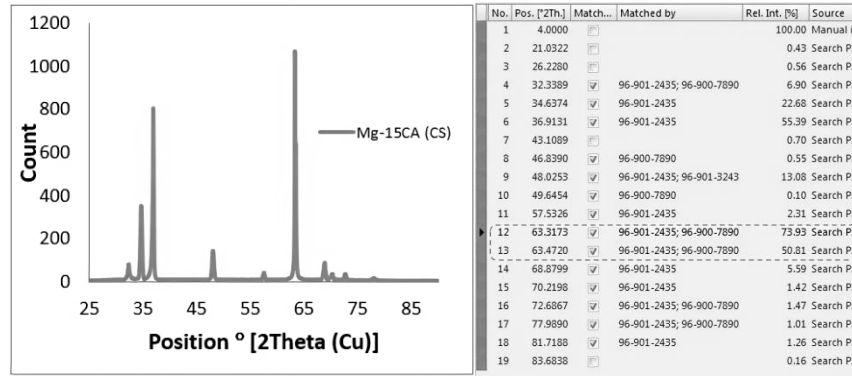


FIGURE 2. Mg-15CA (CS) XRD spectrum and its peak list relating to the elements or phases of Mg, MgO, and CO₂

CA is spread over grain boundaries. The addition of CA and the increase in its content cause the grain boundaries of Mg-xCA to be wider than the grain

boundaries of pure Mg rods. The dark region indicates the presence of CA. There is indicated CA agglomeration with an increase in CA content, especially in Mg-15CA.

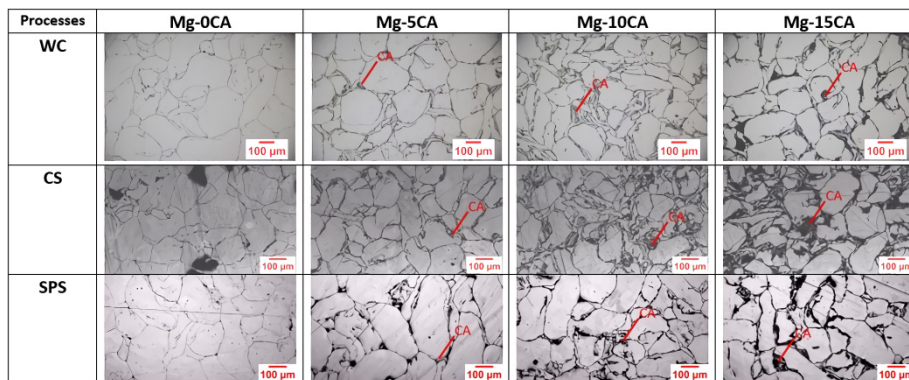


FIGURE 3. The microstructure (OM) of Mg-xCA after being sintered with CS and SPS. Mg-xCA (before CS or as warm compaction results) microstructure is used as a comparison

SEM-EDS-MAPPING OBSERVATION

Figure 4 (SEM-EDS-Mapping results) shows a clear difference in oxygen element content on the overall grain boundary of Mg-xCA (CS and SPS results). Oxygen content is indicated by color, which is blue (for CS) and green (for SPS). On Mg-xCA (CS), oxygen concentrations are found in grain boundaries with a contrasting dark blue color and are also scattered in the Mg matrix (light blue). While on Mg-xCA (SPS), dominant oxygen is concentrated in grain boundaries with much less content compared to Mg-xCA (CS) (the green color does not contrast).

The greater the CA content, the higher the oxygen element content. The oxygen content on the overall area of the Mg-xCA (CS) ranges from 9.1-20.1% wt (Figures 4 & 5). While the oxygen element content of Mg-xCA (SPS) ranges from 3.5-4.8% wt. The lowest value is Mg-15CA (SPS) at 3.5% wt. oxygen.

The oxygen content of Mg-xCA (CS) is much higher than that of Mg-xCA (SPS). Its difference ranges from 1.3-4.7 times, respectively, in the composition $x = 0, 5, 10$ and 15% wt CA. The increasing content of the oxygen element in Mg-xCA CS results compared to the SPS results is supporting evidence that there has been decarbonization

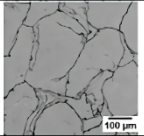
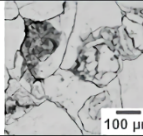
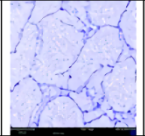
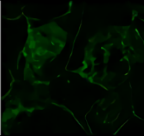
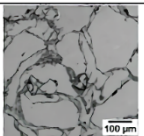
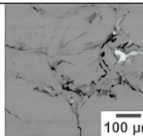
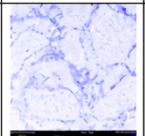
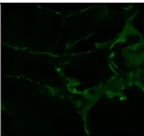
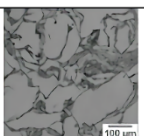
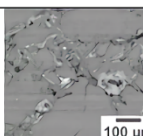
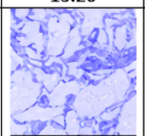
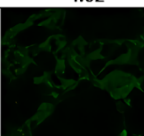
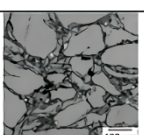
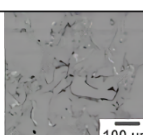
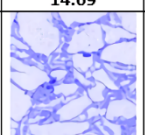
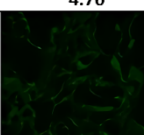
Element SINTERING PROCESS	Overall		O	
	CS	SPS	CS	SPS
Mg-0CA				
% wt			9.14	3.92
Mg-5CA				
% wt			13.26	4.62
Mg-10CA				
% wt			14.69	4.76
Mg-15CA				
% wt			20.12	3.52

FIGURE 4. Images of SEM-EDS-Mapping on the overall area of the Mg-xCA (CS and SPS results), particularly oxygen (O) content

Oxygen content is indicated by dark blue and light blue color for CS and green color for SPS

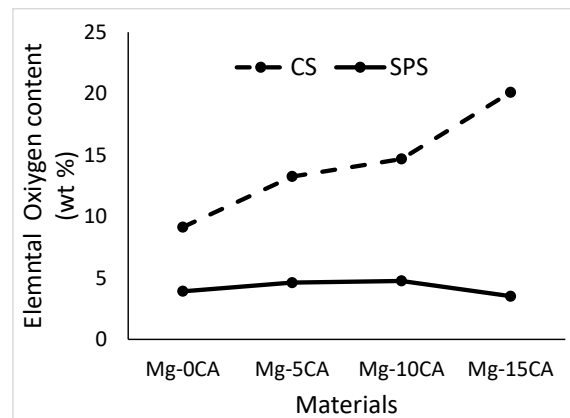


FIGURE 5. Graph of changes in oxygen content on overall area Mg-xCA (CS and SPS results)

of CO_3^{2-} in CA to CO_2 and the formation of MgO. The appearance of CO_2 and MgO further reduces the relative density of Mg-xCA composites. It even reduces the hardness value, especially in Mg-15CA (CS).

MICROHARDNESS (HV)

Hardness of Mg-xCA after being sintered with CS and SPS can be seen in Figure 6. The value of hardness before sintering (WC) is used as a comparison.

Materials	Hv		
	WC	CS	SPS
Mg-0CA	31.9±0.7	30.7±1.6	33.5±1.7
Mg-5CA	32.9±1.2	37.5±2.8	37.1±2.3
Mg-10CA	36.0±2.4	41.1±2.0	38.5±1.7
Mg-15CA	39.1±0.6	37.6±2.9	40.0±1.4

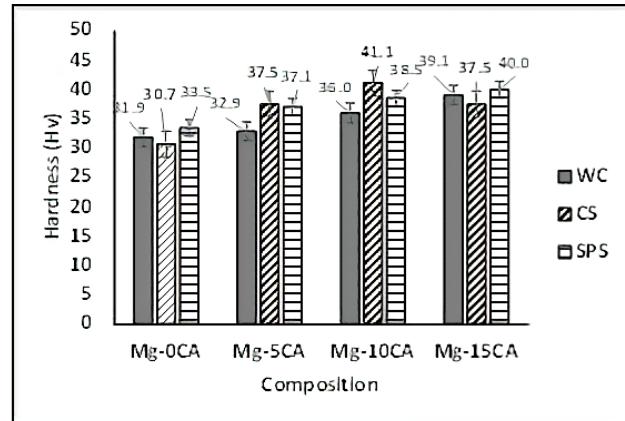


FIGURE 6. Bar chart of Mg-xCA hardness after sintering with CS and SPS

The sintering process tends to increase the hardness of Mg-xCA, especially SPS (Figure 6). Increased hardness of 2-13% (SPS) compared to the condition before sintering (WC) with the same composition. However, some CS results have decreased hardness, where the range is -4-14%, especially Mg-15CA.

Besides, the addition and increase of CA content tends to increase the hardness. The presence of CA reinforcing particles at the grain boundaries inhibits the movement of dislocations between Mg particles so that their hardness increases. The trend of increasing hardness is in line with other previous studies on the fabrication of Mg-HA (variations 0, 5, 10, and 5% by weight of HA) through a combination of powder metallurgy (PM) with microwave sintering, each around 44±1, 58±2, 64±2 and 74±2 Hv (Xiong et al. 2016), as well as the combination of PM with extrusion, each around 49±1, 53±1, 58±1, 61±1 Hv (Del Campo et al. 2014).

The difference in the achievement of the hardness value is suspected to be a factor influencing the initial condition of the raw material. The sizes of the Mg and HA powders were smaller than the sizes of the Mg and CA powders in this study. In the study of fabrication using microwave sintering, the powder sizes were Mg (40 µm) and HA (20 µm) (Xiong et al. 2016), while in extrusion fabrication were Mg (<45 µm) and HA (150 µm) (Del Campo et al. 2014). Meanwhile, in this study, the powder sizes were Mg (60-300 µm) and CA (70 m).

In contrast to Mg-xCA (SPS), there is an anomaly of decreasing hardness with increasing CA content in Mg-xCA (CS), especially in Mg-15CA. In the SPS process, the hardness is at least 33.5 Hv at Mg-0CA and continues to rise to 40.0 Hv at Mg-15CA. Whereas in the CS process the increase in hardness only occurs up to the Mg-10CA composition, then the hardness drops again at Mg-15CA from 41.1 Hv to 37.6 Hv. This can happen because

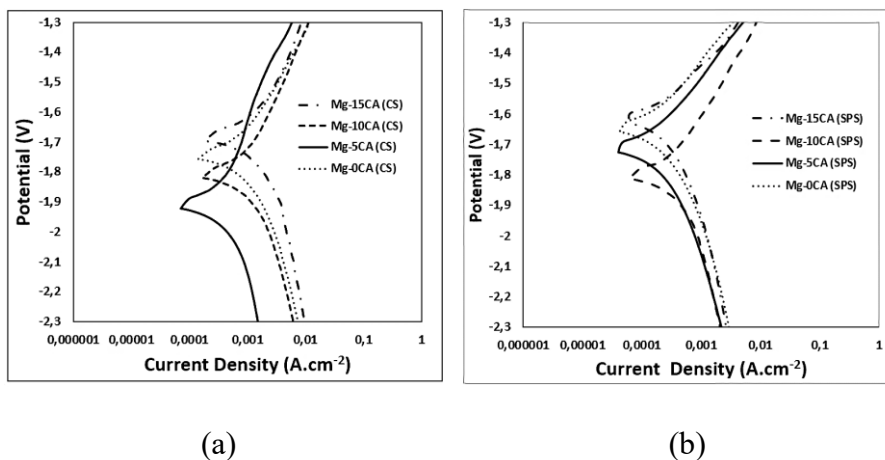


FIGURE 7. Mg-xCA potentiodynamic polarization curves after being sintered with: (a) CS and (b) SPS

carbonate (CO_3^{2-}) in CA breaks down into CO_2 and a small portion of Mg into MgO. From the results of SEM-EDS and mapping, it is seen that there is a significant increase in oxygen elements. This condition can weaken the CA strengthening and powder bond strength.

Potentiodynamic polarization curves of Mg-xCA after sintering with CS and SPS respectively can be seen in Figure 7.

TABLE 2. Current density (I_{corr}) and Corrosion Rate (CR) of Mg-xCA after being sintered with CS and SPS. Mg-xCA before sintering (WC) is used as a comparison

Materials	Current density (Acm^{-2})			Corrosion rate (mm/y)		
	WC	CS	SPS	WC	CS	SPS
Mg-0CA	6.585E-04	6.559E-04	3.929E-04	15.1	15.0	9.0
Mg-5CA	3.087E-04	2.164E-04	2.020E-04	6.9	4.8	4.5
Mg-10CA	4.177E-04	7.803E-04	2.826E-04	9.1	17.1	6.2
Mg-15CA	5.812E-04	1.146E-03	2.978E-04	12.4	24.4	6.4

Figure 7 and Table 2 show that there are significant differences in the degradation characteristics of Mg-xCA from the results of SPS and CS sintering compared to before sintering (WC). The current density and corrosion rate (CR) of Mg-xCA (SPS) are lower than Mg-xCA (CS). There is a significant decrease in current density and corrosion rate of Mg-xCA (SPS), ranging from 32-49% (Table 2). Mg-5CA (SPS) has the lowest values, respectively, $2.02\text{E-}04 \text{ Acm}^{-2}$ (current density) or 4.5 mm/y (CR), while Mg-5CA (CS) is $2.164\text{E-}04 \text{ Acm}^{-2}$ (current density) or 4.8 mm/y (CR). However, some Mg-xCA (CS) actually increased its corrosion rate, particularly in Mg-15CA by 97% from 12.4 to 24.4 mm/y. This phenomenon is in line with CS and SPS studies on Mg-10HA, where there was a decrease in Mg ion release from 85% (CS) to 45% (SPS) after 28 days of immersion in SBF (Khodaei et al. 2020).

The addition of CA tends to decrease its CR compared to CR of Mg-0CA, but CR returns to increase along with the increase of CA content in Mg composites. The same phenomenon also occurs in current density. In the SPS process, the highest CR is at Mg-15CA (6.4 mm/y), up 42.2% compared to CR of Mg-5CA. While in the CS process, the highest CR is at Mg-15CA (24.4 mm/y) or rise to 4 times the CR of Mg-5CA. When compared with Mg-15CA (SPS), its increase is around 2.8 times.

The phenomenon of decreasing CR due to the addition of reinforcement in Mg composites was

reported by several previous studies, such as the Mg-xHA microwave sintering study (Xiong et al. 2016), where the lowest CR in SBF solution was 2.09 mm/yr or $1\text{E-}04 \text{ Acm}^{-2}$ (for current density) at Mg-10HA, but at Mg-15CA the CR increased again to 3.52 mm/y or $1.77\text{E-}04 \text{ Acm}^{-2}$ (for current density). Meanwhile, it was reported that the results of the double sintered Mg-3Zn-xHA study ($x=0, 2, 5, 10\%$) had the lowest CR of 1.17 mm/y in Mg-3Zn-5CA (Jaiswal et al. 2018). In the study of lamellar Mg-xHA SPS ($x = 0, 8, 10$ and 15%) it was reported that the lowest CR in 3.5% NaCl solution was 5.44 mm/y at Mg-10HA (Sunil et al. 2014). The greater the HA content, the greater the possibility for agglomeration to occur, so that it can function as a second phase which accelerates the rate of degradation.

In the CS process, CO_2 gas resulting from carbonate decomposition can be trapped between Mg-xCA grains and forming microporosity, thereby reducing density. Evidently, there is a significant reduction in relative density, particularly in Mg-15CA (CS). This density decrease causes the corrosion rate (CR) to increase again through the mechanism of intergranular corrosion or in combination with pitting corrosion. Besides that, the presence of CO_2 tends to increase the acidity of the solution and trigger sweet corrosion through the mechanism of pitting corrosion (Mahmoud Abbas et al. 2012; Yunita & Siska Titik 2015). In the SPS process, the CO_2 and MgO formed can be minimized and the resulting relative density is better, so that the current density and CR are lower.

CONCLUSION

In this research, the sintering process has been conducted on Mg-xCA with conventional sintered (CS) and spark plasma sintering (SPS). The SPS process is considered appropriate and effective for the further compaction of Mg-xCA with sinter than the CS process. The SPS process can minimize the formation of other elements or phases, particularly to prevent decomposition (CO_3^{2-}) on CA into CO_2 gas. Overall, the relative density is better, the hardness increases, and the corrosion rate decreases. The process is short with heating focused on the Mg-xCA particle interface, clean with a controlled chamber condition, and the compaction process simultaneously takes place so that SPS becomes the best choice in the Mg-xCA sintered process compared to the CS process. Besides, the addition and increase of CA content decreases the relative density and increases the hardness. The addition of CA to Mg-xCA also inhibits the corrosion rate, particularly in Mg-5CA, but the higher CA content (10 and 15% wt) again increases the corrosion rate.

ACKNOWLEDGEMENTS

This research was supported by the PDD research grant (contract number 8/E1/KP.PTNBH/2020 and 255/PKS/R/UI/2020 dated March 19, 2020 and NKB-414/UN2.RST/HKP.05.00/2020) from the Ministry of Research, Technology and Higher Education of the Republic of Indonesia. The author would like to thank the Director of the Center for Material Technology -BPPT-Indonesia, P2 Fisika-LIPI for the support of several types of equipment for research and testing.

REFERENCES

- Ahmad Jabir Rahyussalim, Aldo Fransiskus Marsetio, Achmad Fauzi Kamal, Sugeng Supriadi, Iwan Setyadi, Pancar Muhammad Pribadi, Wildan Mubarak & Tri Kurniawati. 2021. Synthesis, structural characterization, degradation rate, and biocompatibility of magnesium-carbonate apatite (Mg-Co₃Ap) composite and its potential as biodegradable orthopaedic implant base material. *Journal of Nanomaterials* 2021: 6615614. <https://doi.org/10.1155/2021/6615614>.
- Ahmad Jabir Rahyussalim, Sugeng Supriadi, Achmad Fauzi Kamal, Aldo Fransiskus Marsetio & Pancar Muhammad Pribadi. 2019. Magnesium-carbonate apatite metal composite: Potential biodegradable material for orthopaedic implant. In *AIP Conference Proceedings* 2092: 20021. AIP Publishing LLC. <https://doi.org/10.1063/1.5096689>.
- Annur, D. 2017. Powder metallurgy preparation of Mg-Ca Alloy for biodegradable implant application to. *Journal of Physics: IOP Conference Series* 817. <https://doi.org/10.1088/1742-6596/817/1/012062>.
- Ayukawa Yasunori, Yumiko Suzuki, Kanji Tsuru, Kiyoshi Koyano & Kunio Ishikawa. 2015. Histological comparison in rats between carbonate apatite fabricated from gypsum and sintered hydroxyapatite on bone remodeling. *BioMed Research International* <https://doi.org/10.1155/2015/579541>.
- ASTM E384-17. 2017. *Standard Test Method for Microindentation Hardness of Materials*.
- ASTM. G102-89. 2015. *Standard Practice for Calculation of Corrosion Rates and Related Information from Electrochemical Measurements*.
- ASTM. G5-94. 2014. *Standard Reference Test Method for Making Potentiodynamic Anodic Polarization Measurements*.
- Atmaja Surbakti, Maximillian Ch. Oley & Eko Prasetyo. 2017. Perbandingan antara penggunaan karbonat apatit dan hidroksi apatit pada proses penutupan defek kalvaria dengan menggunakan plasma kaya trombosit. *Jurnal Biomedik (Jbm)* 9(2): 107-114. <https://doi.org/10.35790/jbm.9.2.2017.16359>.
- Center for Material Technology (BPPT). 2017. Technical Note GL3/Alkes.
- Del Campo, R., Savoini, B., Muñoz, A., Monge, M.A. & Pareja, R. 2017. Processing and mechanical characteristics of magnesium-hydroxyapatite metal matrix biocomposites. *Journal of the Mechanical Behavior of Biomedical Materials* 69: 135-143. <https://doi.org/10.1016/j.jmbm.2016.12.023>.
- Del Campo, R., Savoini, B., Muñoz, A., Monge, M.A. & Garcés, G. 2014. Mechanical properties and corrosion behavior of Mg-HAP composites. *Journal of the Mechanical Behavior of Biomedical Materials* 39: 238-246. <https://doi.org/10.1016/j.jmbm.2014.07.014>.
- Doi, Y., Koda, T., Adachi, M., Wakamatsu, N., Goto, T., Kamemizu, H., Moriwaki, Y. & Suwa, Y. 1995. Pyrolysis-gas chromatography of carbonate apatites used for sintering. *Journal of Biomedical Materials Research* 29(11): 1451-1457. <https://doi.org/10.1002/jbm.820291117>.
- Godavitarne, C., Robertson, A., Peters, J. & Rogers, B. 2017. Biodegradable materials. *Orthopaedics and Trauma* 31(5): 316-320. <https://doi.org/10.1016/j.mporth.2017.07.011>.
- Gu, X-N. & Zheng, Y-F. 2010. A review on magnesium alloys as biodegradable materials. *Frontiers of Materials Science in China* 4(2): 111-115. <https://doi.org/10.1007/s11706-010-0024-1>.
- Gu, X., Zhou, W., Zheng, Y., Dong, L., Xi, Y. & Chai, D. 2010. Microstructure, mechanical property, bio-corrosion and cytotoxicity evaluations of Mg/HA composites. *Materials Science and Engineering: C* 30(6): 827-832. <https://doi.org/10.1016/j.msec.2010.03.016>.
- Haghshenas, M. 2017. Mechanical characteristics of biodegradable magnesium matrix composites: A review. *Journal of Magnesium and Alloys* 5(2): 189-201. <https://doi.org/10.1016/j.jma.2017.05.001>.
- Hirokazu Nagai, Masako Kobayashi-Fujioka, Kenji Fujisawa, Go Ohe, Natsumi Takamaru, Kanae Hara, Daisuke Uchida, Tetsuya Tamatani, Kunio Ishikawa & Youji Miyamoto. 2015.

- Effects of low crystalline carbonate apatite on proliferation and osteoblastic differentiation of human bone marrow cells. *Journal of Materials Science: Materials in Medicine* 26(2): 1-8. <https://doi.org/10.1007/s10856-015-5431-5>.
- Ishikawa, K. 2019. Carbonate apatite bone replacement: Learn from the bone. *Journal of the Ceramic Society of Japan* 127(9): 595-601. <https://doi.org/10.2109/jcersj2.19042>.
- Iwan Setyadi, Aldo Fransiskus Marsetio, Achmad Fauzi Kamal, Rahyussalim, Sugeng Supriadi & Bambang Suharno. 2020a. Microstructure and microhardness of carbonate apatite particle-reinforced Mg composite consolidated by warm compaction for biodegradable implant application. *Materials Research Express* 7(5). <https://doi.org/10.1088/2053-1591/ab7d70>.
- Iwan Setyadi, Pancar Muhammad Pribadi, Aldo Fransiskus Marsetio, Achmad Fauzi Kamal, Rahyusalim, Bambang Suharno & Sugeng Supriadi. 2020b. Characteristics investigation of the initial development of miniplate made from composite of magnesium/carbonate apatite fabricated by powder metallurgy method for biodegradable implant applications. In *Key Engineering Materials* 833 KEM: 194-198. Trans Tech Publications Ltd. <https://doi.org/10.4028/www.scientific.net/KEM.833.194>.
- Jaiswal, S., Manoj Kumar, R., Gupta, P., Kumaraswamy, M., Roy, P. & Lahiri, D. 2018. Mechanical, corrosion and biocompatibility behaviour of Mg-3Zn-HA biodegradable composites for orthopaedic fixture accessories. *Journal of the Mechanical Behavior of Biomedical Materials* 78: 442-454. <https://doi.org/10.1016/j.jmbbm.2017.11.030>.
- Kingston Technical Software. n.d. *Corrosion Rate Conversion*. <https://www.corrosion-doctors.org/Principles/Conversion.htm>.
- Kokubo, T., Kushitani, H., Sakka, S., Kitsugi, T. & Yamamuro, T. 1990. Solutions able to reproduce *in vivo* surface-structure changes in bioactive glass-ceramic A-W3. *Journal of Biomedical Materials Research* 24(6): 721-734. <https://doi.org/10.1002/jbm.820240607>.
- Kuśnierczyk, K. & Basista, M. 2017. Recent advances in research on magnesium alloys and magnesium-calcium phosphate composites as biodegradable implant materials. *Journal of Biomaterials Applications* 31(6): 878-900. <https://doi.org/10.1177/0885328216657271>.
- Landi, E., Celotti, G., Logroscino, G. & Tampieri, A. 2003. Carbonated hydroxyapatite as bone substitute. *Journal of the European Ceramic Society* 23(15): 2931-2937. [https://doi.org/10.1016/S0955-2219\(03\)00304-2](https://doi.org/10.1016/S0955-2219(03)00304-2).
- Linhart, W., Peters, F., Lehmann, W., Schwarz, K., Schilling, A.F., Amling, M., Rueger, J.M. & Epple, M. 2000. Biologically and chemically optimized composites of carbonated apatite and polyglycolide as bone substitution materials. *J. Biomed. Mater. Res.* 54(2): 162-171.
- Liu, R., Wang, W., Chen, H., Lu, Z., Zhao, W. & Zhang, T. 2019. Densification of pure magnesium by spark plasma sintering-discussion of sintering mechanism. *Advanced Powder Technology* 30(11): 2649-2658. <https://doi.org/10.1016/j.apt.2019.08.012>.
- Madupalli, H., Pavan, B. & Tecklenburg, M.M.J. 2017. Carbonate substitution in the mineral component of bone: Discriminating the structural changes, simultaneously imposed by carbonate in A and B sites of apatite. *Journal of Solid State Chemistry* 255: 27-35. <https://doi.org/10.1016/j.jssc.2017.07.025>.
- Masayuki Kanazawa, Kanji Tsuru, Naoyuki Fukuda, Yuta Sakemi, Yasuharu Nakashima & Kunio Ishikawa. 2017. Evaluation of carbonate apatite blocks fabricated from dicalcium phosphate dihydrate blocks for reconstruction of rabbit femoral and tibial defects. *Journal of Materials Science: Materials in Medicine* 28(6): 85. <https://doi.org/10.1007/s10856-017-5896-5>.
- Mohammad Khodaei, Farahnaz Nejatidaneh, Mohammad Javad Shirani, Srinivasan Iyengar, Hossein Sina & Omid Savabi. 2020. Magnesium/nano-hydroxyapatite composite for bone reconstruction: The effect of processing method. *Journal of Bionic Engineering* 17(1): 92-99. <https://doi.org/10.1007/s42235-020-0007-6>.
- Mahmoud Abbas Ibraheem, Abd El Aziz El Sayed Fouda, Mohamed Talaat Rashad & Fawzy Nagy Sabbahy. 2012. Sweet corrosion inhibition on API 5L-B pipeline steel. *International Scholarly Research Notices* 2012: 892385. <https://doi.org/10.5402/2012/892385>.
- NN n.d. *Spark Plasma Sintering*. http://www.subtech.com/dokuwiki/doku.php?id=spark_plasma_sintering. Accessed on December 3, 2019.
- Radha, R. & Sreekanth, D. 2017. Insight of magnesium alloys and composites for orthopedic implant applications - A review. *Journal of Magnesium and Alloys* 5(3): 286-312. <https://doi.org/10.1016/j.jma.2017.08.003>.
- Siska Wiwanto, Lilies Dwi Sulistyani, Fourier Dzar Eljabbar Latief, Sugeng Supriadi, Bambang Pontjo Priosoeryanto & Benny Syariefsyah Latief. 2018. The experiment of magnesium ECAP miniplate as alternative biodegradable material (on male white New Zealand rabbits). In *AIP Conference Proceedings*, 1933: 20013. AIP Publishing LLC. <https://doi.org/10.1063/1.5023947>.
- Sunil, B.R., Ganapathy, C., Sampath Kumar, T.S. & Chakkingal, U. 2014. Processing and mechanical behavior of lamellar structured degradable magnesium-Hydroxyapatite implants. *Journal of the Mechanical Behavior of Biomedical Materials* 40: 178-189. <https://doi.org/10.1016/j.jmbbm.2014.08.016>.
- Supriadi, S., Kristianto, H., Whulanza, Y., Saragih, A.S., Dhelika, R., Latief, B.S. & Taufiq, T. 2018. Fabrication of magnesium ECAP based maxillary miniplate-typed implant through the method of micro forming. *IOP Conference Series: Materials Science and Engineering* 432: 012037. <https://doi.org/10.1088/1757-899X/432/1/012037>.
- Witte, F., Feyerabend, F., Maier, P., Fischer, J., Störmer, M., Blawert, C., Dietzel, W. & Hort, N. 2007. Biodegradable magnesium-Hydroxyapatite metal matrix composites. *Biomaterials* 28(13): 2163-2174. <https://doi.org/10.1016/j.biomaterials.2006.12.027>.

- Xiong, G., Nie, Y., Ji, D., Li, J., Li, C., Li, W., Zhu, Y., Luo, H. & Wan, Y. 2016. Characterization of biomedical hydroxyapatite/magnesium composites prepared by powder metallurgy assisted with microwave sintering. *Current Applied Physics* 16(8): 830-836. <https://doi.org/10.1016/j.cap.2016.05.004>.
- Youness, R.A., Taha, M.A. & Ibrahim, M.A. 2017. Effect of sintering temperatures on the *in vitro* bioactivity, molecular structure and mechanical properties of titanium/carbonated hydroxyapatite nanobiocomposites. *Journal of Molecular Structure* 1150: 188-195. <https://doi.org/10.1016/j.molstruc.2017.08.070>.
- Yunita Sari & Siska Titik Dwiwati. 2015. Korosi H₂S dan CO₂ pada peralatan statik di industri minyak dan gas. *Jurnal Konversi Energi dan Manufaktur UNJ* 2(1): 18-22.
- Zheng, Y.F., Gu, X.N. & Witte, F. 2014. Biodegradable metals. *Materials Science and Engineering: R: Reports* 77: 1-34. <https://doi.org/10.1016/j.mser.2014.01.001>.

*Corresponding author; email: ilsetyadi2810@gmail.com